Supplementary Material for

The global tree restoration potential

Jean-Francois Bastin*, Yelena Finegold, Claude Garcia, Danilo Mollicone, Marcelo Rezende, Devin Routh, Constantin M. Zohner, Thomas W. Crowther

*Corresponding author. Email: bastin.jf@gmail.com

Published 5 July 2019, *Science* **365**, 76 (2019)
DOI: 10.1126/science.aax0848

This PDF file includes:

Materials and Methods
Figs. S1 to S12
Tables S1 to S3
References

Other Supplementary Material for this manuscript includes the following:
(available at science.sciencemag.org/content/365/6448/76/suppl/DC1)

Data Files S1 and S2 as separate Excel files

Materials and Methods

Tree cover

To assess the global potential tree cover, we first measured the tree cover of 78,774 0.5-hectare plots distributed throughout the global protected regions of the world (i.e. in regions with limited human activity) following a systematic sampling grid design (20-by-20km), using the augmented visual interpretation approach(*8*) followed by Bastin and colleagues (2017)(*13*). For analysis, we used all dryland plots in protected areas assessed in ref (9) (N=23,042), and collected new plots for all other biomes (N=34,564) following the same procedure. In addition, we added plots from the global dryland assessment(*8*) falling in desert regions to cover the full range of environmental conditions.

Augmented visual interpretation of tree cover with Collect Earth

The assessment of tree cover in each plot was performed through the Augmented Visual Interpretation approach(*8*), using Collect Earth. Collect Earth is an open access software built on Google Earth and Google Earth Engine and developed by the Open Foris initiative of the Food and Agriculture Organization of the United Nations (FAO). Collect Earth allows the operator to photo-interpret the tree cover of a plot (here a square of 70-by-70m) combining land cover information gathered from satellite images with very high spatial (pixel size ≤ 1metre) and temporal resolution (daily data acquisition)(*8*). The operator photo-interprets very high spatial resolution satellite images(*8*), made freely accessible for visualization on Google Earth, and in parallel controls his measurements with spectral information, automatically compiled for the last 20 years from medium-to-high resolution satellite images, in particular from MODIS and Landsat7/8. Each plot presents a systematic grid of 7-by-7 points (49 points) allowing easy and direct measurements of tree canopy cover, with each point representing 2% of the plot. The fundamental variable measured in this study was the percentage of tree cover, ranging from 0 to 100%.

Regions with limited human activity

To identify the regions of the world with limited human activity, we used the World Database on Protected Areas(*9*) (WDPA; Fig. S2), developed by the United Nations Environmental Program (UNEP) and the International Union for Conservation of Nature (IUCN). The WDPA is the most comprehensive global database of marine and terrestrial protected areas, and includes a whole suite of descriptors (e.g. status of protection, year of establishment, etc) that were not incorporated into the present study. Here, we accounted for all protected areas available with the intention to maximize the number of training points used for the model. These regions are not entirely exempt from human activity(*11*), but these ecosystems represent areas where humans have had minimal impacts on the overall ecosystem type or forest cover. Assuming that any human effects will be likely to reduce tree cover, our modeled estimates are likely to be conservative estimates of potential tree cover.

Environmental drivers

To predict the global potential tree cover, we first selected the most relevant environmental covariates from a set of 58 environmental variables, comprising soil, topographic and climate layers (Data S2). All covariate layers were resampled and reapplied to a unified Eckert 4 equal area projection, at 30 arc-seconds resolution (≈1km at the equator). Layers with a higher original

pixel resolution were downsampled using a mean aggregation method; layers with a lower original resolution were resampled using simple upsampling (i.e., without interpolation) to align with the higher resolution grid. In total, this corresponds to 34 quantitative soil descriptors extracted from gridsoils(*22*), 5 topographic properties extracted from GMTED2010 and 19 bioclimatic variables extracted from Worldclim 2.0(*23*). We then used the ClustOfVar R package to cluster the covariates in groups of collinear variables representative of environmental variations among the 78,774 plots. This resulted in the selection of 5 climate, 3 soil and 2 topographic variables: annual mean temperature; annual precipitation; precipitation seasonality; mean temperature of the wettest quarter; precipitation of the driest quarter; organic carbon stock from 0-to-15 cm, depth to bedrock; sand content from 0-to-15 cm; elevation; and hillshade.

Predicting the potential tree cover

We implemented the 10 selected variables in a random forest machine learning regression model(*12*) to predict the tree cover among the 78,774 plots (number of trees: 20) (see Notes). The model is built by finding of the set of combinations of covariates that predict best the training samples (*12*). This machine learning approach allows us to generate robust predictions without requiring explicit instruction or hypothesis when building the model. The quality of the model was tested and validated using a k-fold cross-validation method; where k (k=5) models were trained from k subsets of the original data (total number of plots minus the total number of plots divided by k) and tested on k subsets of remaining independent data (total number of plots divided by k). Combining the k iterations, we compared the original full dataset with the complete set of remaining independent data. The modelling approach was then validated by regressing predicted (x-axis) vs observed values (y-axis), following Pineiro and colleagues (2008)(*24*). The model had high predictive power (R2=0.86, intercept=-2.05% tree cover; slope=1.06; Fig. S3) and the k-fold cross validation revealed that our model could explain over 71% of the variation in tree cover without bias (intercept=0.34% tree cover; slope=0.99; Fig. S4). The potential tree cover was then spatially extrapolated outside protected areas for each pixel using model coefficients combining the 10 selected variables information.

Potential tree cover, forest extent and corresponding areas for restoration

Forest cover

The fundamental variable predicted in this study was the percentage of tree cover per pixel. To estimate the potential area of forest, we converted the global potential tree cover in forest/non-forest classes using the latest definition of forest from the Forest Resources Assessment report of the Food and Agriculture Organization of the United Nations(*14*). Each pixel presenting at least 10% of tree cover was assigned as a forest. Each pixel presenting less than 10% of tree cover was assigned as a non-forest (Fig. S7). We then used the function area from the raster R package to calculate the area of each pixel and we summed the total area covered by pixels assigned as a forest. We then calculated the potential area of forest around the globe, by country and by ecoregion, as defined by the World Wide Fund for Nature (WWF) in the shapefiles provided by The Nature Conservancy (Fig. S7).

Forest area available for restoration

To provide an estimate of the total area available for forest restoration we subtracted the current estimation of forest extent (calculated from the tree cover map published by Hansen and colleagues in 2013(*15*)) to the global potential forest extent (compiled from our global potential

tree cover map- Fig. 2A). To provide realistic numbers, we also removed all areas presenting urban settlements or agricultural activities, as identified in the global land cover map of the European Space Agency(*16*), Globcover (i.e. removing the following classes: 11,14,20,30,190). It should be noted that these classes contain from 20 to 100% of crops per pixel, meaning the smallest area covered by crops is equal to 1.8 hectare (Fig. S7B). We kept grazing areas, as several studies suggest alternatives to improve the efficiency of livestock production (*7*,*25*).
To provide an additional assessment of the potential forest restoration, we re-did the same round of calculation, replacing, for the assessment of agricultural activites, the Globcover layer by the percentage of cropland per pixel published by Fritz and colleagues in 2015 (*18*) (Fig. S7C). The percentage of cropland ranges from 0 to 100% per pixel of 1 km2, meaning the smallest area covered by crops is equal to 1 hectare.

Canopy cover

To provide a better assessment of the global restoration potential, we evaluated the potential "canopy cover". We refer to the "canopy cover" as the sum of tree crown area vertically projected to the ground (i.e. 1% of tree cover over 1ha corresponding to a canopy cover of 0.01ha, and 100% to 1ha; Fig. S8). This simple metric is independent of any tree cover threshold or forest definition, and includes all levels of tree cover of a given region while more appropriately balancing the importance of tree density.

Canopy cover available for restoration

The potential area of continuous tree canopy available for restoration has been calculated with a similar approach as used for the potential restoration area of forest. We subtracted the current tree cover from Hansen and colleagues(*15*) to our estimate of the potential tree cover (Fig. 2B), kept pixels with remaining potential increase in tree cover (whether they present an initial tree cover or not). We then assessed the potential restoration by removing pixels presenting urban settlements or agricultural activities identified in the global land cover map (*16*) (i.e. removing the following classes: 11,14,20,30,190).
To provide an additional assessment of the potential forest restoration, we re-did the same round of calculation, replacing, for the assessment of agricultural activites, the Globcover layer by the percentage of cropland per pixel published by Fritz and colleagues in 2015 (*17*) (Fig. 2C).

Risks of future changes

For the future projections, we re-ran our original model, keeping the 3 soil and 2 topographic variables unchanged and updating the 5 bioclimatic variables from three general circulation models (GCMs) commonly used in ecology(*26*, *27*). Two Community Earth System Models (CESMs) were chosen as they investigate a diverse set of earth-system interactions: the CESM1 BGC (a coupled carbon–climate model accounting for carbon feedback from the land) and the CESM1 CAM5 (a community atmosphere model)(*26*). Additionally, the Earth System component of the Met Office Hadley Centre HadGEM2 model family was used as the third and final model(*27*). To generate the data, we chose Representative Common Pathways 4.5 and 8.5 (RCP 4.5, RCP 8.5) scenarios from the Coupled Model Intercomparison Project Phase 5 (CMIP5) as the input. The RCP 4.5. is a stabilization scenario, meaning that it accounts for a stabilization of radiative forcing before 2100, anticipating the development of new technologies and strategies for reducing greenhouse gas emissions. Generating climate data from the RCP 4.5 anticipates potential change in which the increase of global temperature is limited to 1.5^{o}C by

2050(*1*). The RCP 8.5 corresponds to the 'business as usual' scenario, combining assumptions of high demography increase and slow technological change or energy use efficiency. For each output, a delta downscaling method developed by the CGIAR Research Program on Climate Change, Agriculture and Food Security (CCAFS) was applied to reach a 30 arc-seconds resolution(*28*), using current conditions Worldclim 1.4 as a reference.
From this approach, we produced 6 potential layers, voluntary restricted to the near future, i.e. 2050, one for each RCP (RCP 4.5 and 8.5) and one for each GCM (CESM1 BGC, CESM1 CAM5 and the HadGEM2ES). Future potential tree cover and expected changes in potential tree cover are illustrated for the 6 layers in Fig. S10 and S11.

The risk assessment for changes between current and future tree cover potential was deduced by subtracting the "current potential" from the "future potential" so that potential increases are positive and potential decreases negative. In the main text, we report the change according to the average difference between present and future tree cover potential maps. We show that under RCP 4.5, we risk to lose an equivalent of 177, 175 and 172 Mha of potential canopy cover respectively for CESM1 BGC, CESM1 CAM5 and the HadGEM2ES; and under RCP 8.5 an equivalent of 228, 223 and 220 Mha (Figs. S9,S11). The small variation of these estimates within each scenario shows agreement between the chosen GCMs. The difference between the two scenarios, i.e. between the implementation of mitigation policies and business as usual, represents on average an area of 49 Mha of canopy cover.

Estimation of the potential to restore trees and carbon stocks

We extrapolated the quantity of carbon stocks that could be restored from a combination of our calculations of the potential continuous tree cover available for restoration with numbers from the literature (Table S2). In practice, we used available (biome- or ecoregion-level) reference data and multiplied it with the corresponding continuous tree cover available for restoration. For the carbon stocks we combined the average values of all the information gathered by Pan and colleagues(*18*) for Boreal, Temperate and Tropical biomes, and by Grace and colleagues(*19*) for Drylands. Each value of tree density or carbon density reported in these studies were associated to a pixel-value of potential tree cover of 100%. For example, in the tropics, the carbon density of 282.5 tC.ha-1 reported by Pan and colleagues (2011), is attributed to a pixel when its value of potential tree cover equals 100%. If the potential tree cover of the pixel is equal to 10%, its corresponding potential carbon density equals 23.2 tC.ha-1. The same calculation being done for the tree density. It should be noted that all carbon pools related to forest (aboveground, belowground, dead wood, litter and soil) were accounted for in the numbers of carbon densities.

Error and uncertainties

Interpolation limits

We studied the limits of our predictive model by comparing the range of the 10 environmental values covered by our sampling design (i.e. the 78,774 plots) with their full range across the globe. Using these minima and maxima, we assessed the percentage of interpolation of each pixel. This allows us to differentiate interpolation from extrapolation in our current global potential tree cover map. In total, we observe that our map is extrapolated on average at 8% (Fig. S12).

Uncertainty in the global potential tree cover estimation

We calculated uncertainties of the pixel-based prediction of tree cover and of the global estimate of continuous tree cover from the k tree cover maps produced in the k-fold cross-validation scheme (Figs. S5,6).
By stacking the k predictions of the global potential tree canopy cover and calculating the standard deviation of the k predicted tree canopy cover values for each pixel, we can visualize how the confidence in our model varies across space (Fig. S6). Across all pixels, the mean standard deviation around the modeled estimate is about 9% in tree cover (i.e. 28% of the mean tree cover; Fig. S6). Uncertainties are highest in regions with intermediate levels of tree cover potential (tree cover uncertainty of ~15%; Fig. S5). In contrast, we had high model confidence in non-forested deserts or densely forested regions (tree cover uncertainty <1%; Fig. S6). While such pattern was expected, as "0%" and "100%" of tree cover are two big attractors in our dataset (Fig. S2), we observe that these patterns are systematic across the tropical dense forests. Model simulations for tropical forests in South America and Asia are highly consistent, predicting 100% of tree cover across most of the regions. However, the uncertainty in Africa highlights the possibility for African tropical ecosystems to either exist in a state of dense forest or open land (Figs. S6B,C). This observation lends some support to previous work highlighting the presence of two alternative stable states for forest ecosystems in Africa(*29*).

GCMs uncertainties

Uncertainties related to the choice of the GCM were assessed by calculating the standard deviation of the prediction from the set of three maps produced for each year and each RCP (Fig. S10). Importantly, the choice of the GCM influences less than 5% of the estimated future potential continuous tree cover, showing that all GCMs consistently predict tree cover losses by 2050.
All analysis were performed using Rcran (v.3) and Google Earth Engine Code Editor.

Figures

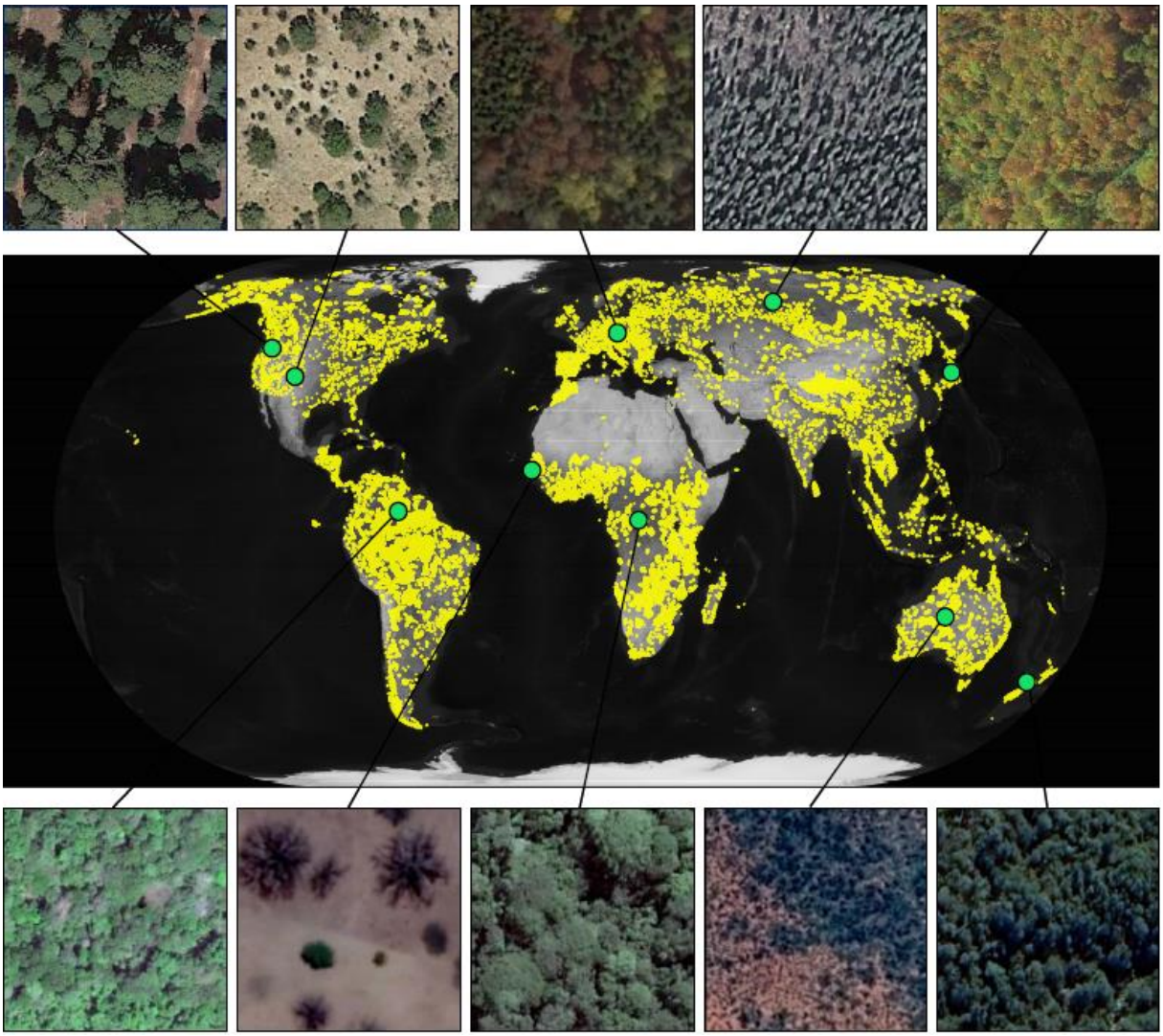

Fig. S1. Observed tree cover across the world's protected areas. Spatial distribution of the 0.5 hectare plots located in protected areas (*9*), for which we photo-interpreted tree cover using very high spatial resolution images. Small captions represent the different forest types in protected areas as seen from very high spatial resolution images, including boreal, dry, temperate and tropical forests.

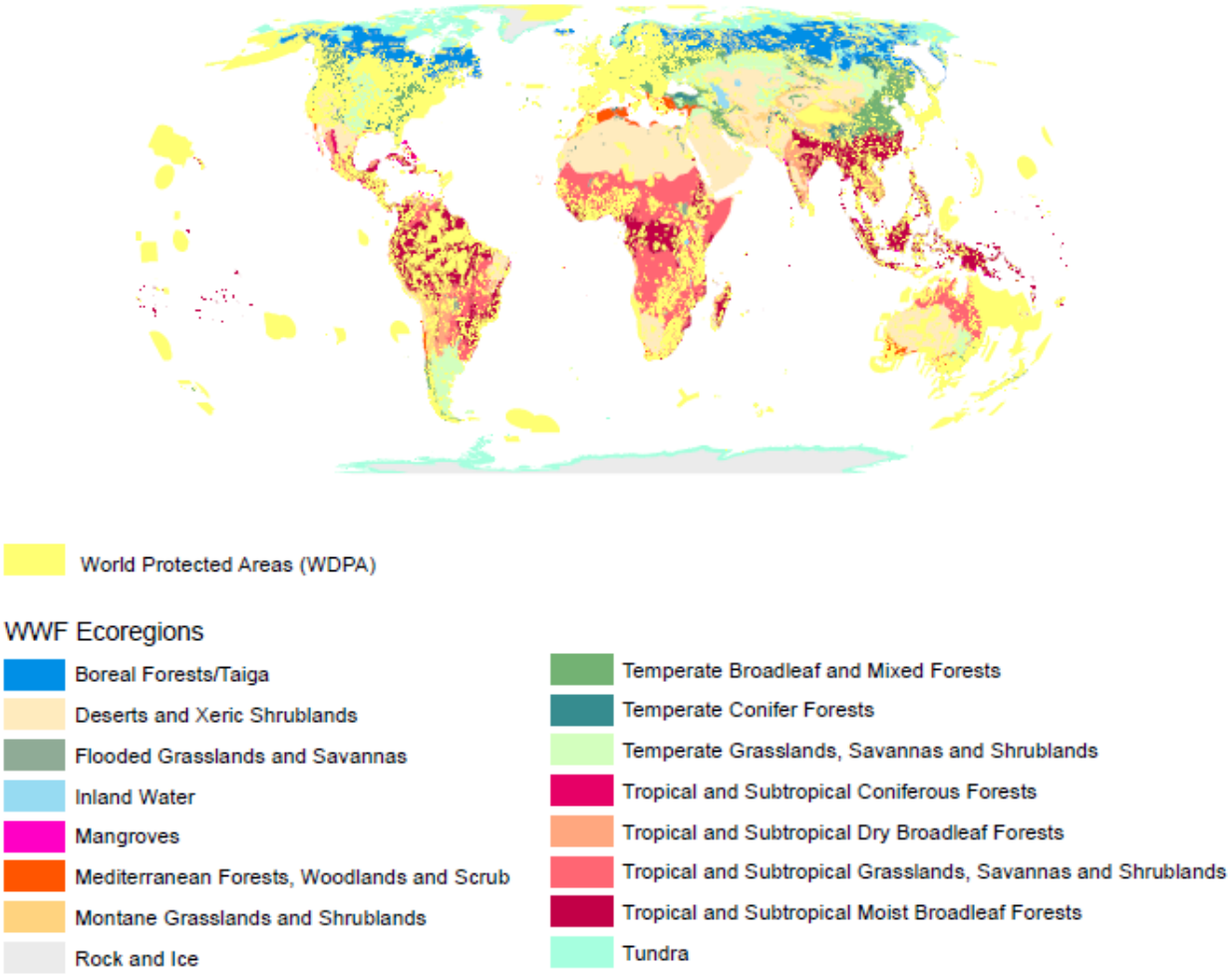

Fig. S2. Distribution of the World's protected areas among the main Ecoregions of the world. The World Database on Protected Areas (WDPA) is developed by the United Nations Environmental Program (UNEP) and the International Union for Conservation of Nature (IUCN). The WDPA is the most comprehensive global database of marine and terrestrial protected areas. The ecoregions of the world are provided by the Nature Conservancy and defined by the World Wide Fund for Nature.

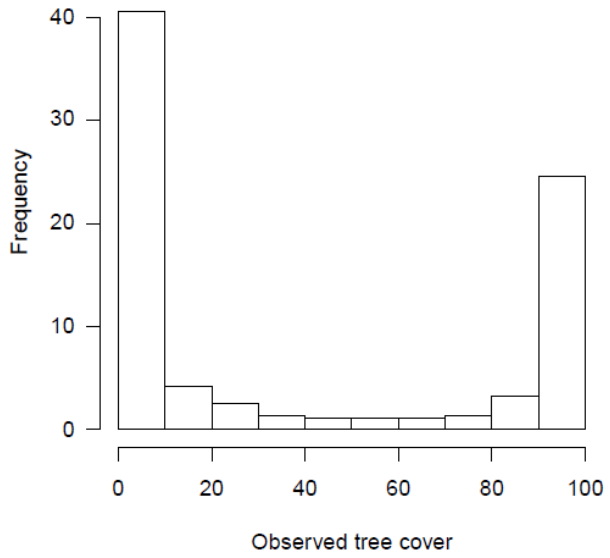

Fig. S3. Tree cover distribution. Histogram illustrating the relative frequency of tree cover, distributed by bins of 10 %. The U-shaped distribution shows a dominance of 0 and 100% of tree cover in the world, when tree cover is photo-interpreted at very high spatial resolution in protected areas, on 0.5-hectare plots and independently of model-based approaches.

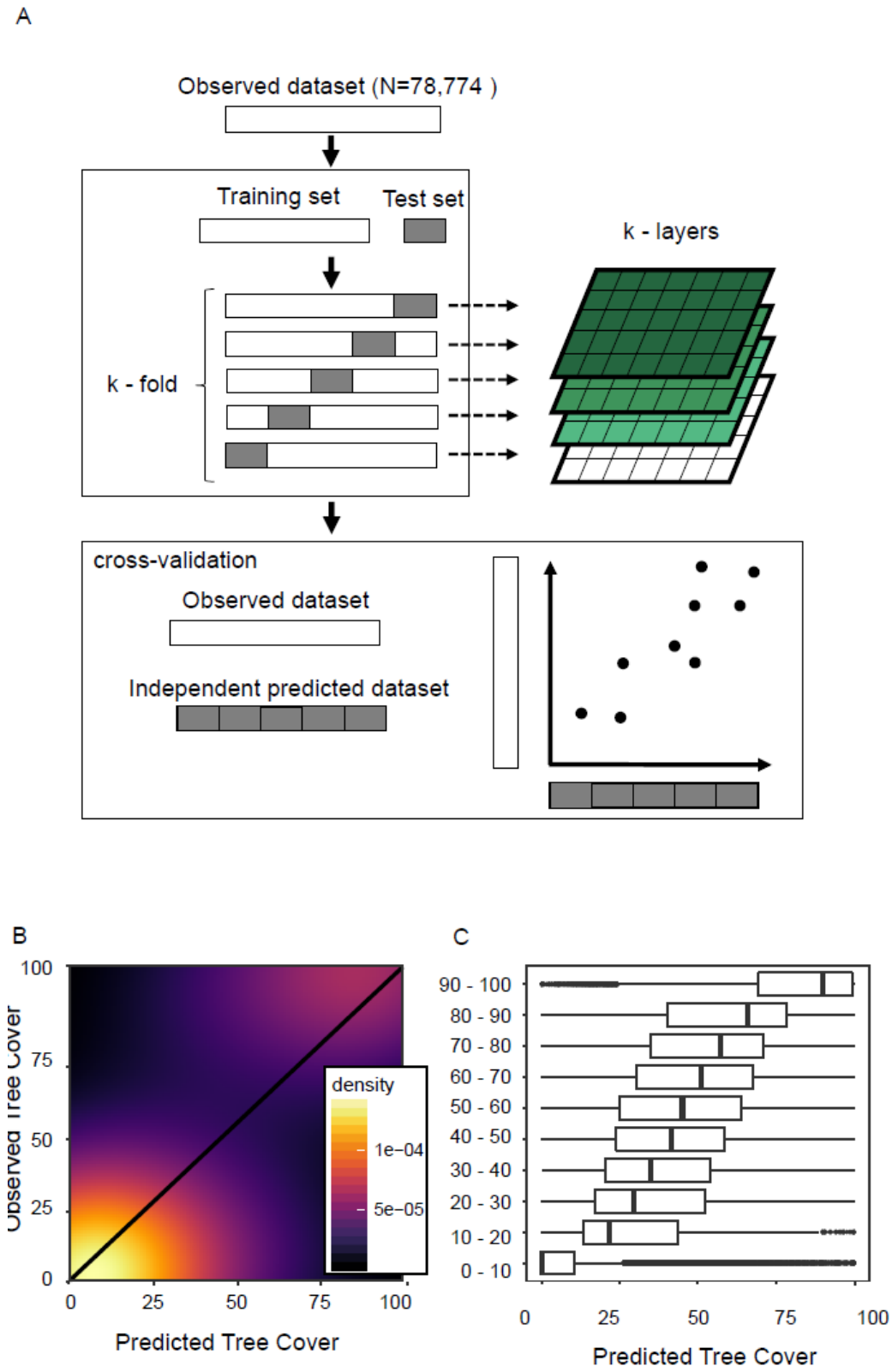

Fig. S4. K-fold cross-validation (A) procedure; (B) density plot and (C) boxplots of observed versus predicted tree cover estimates. See Methods for detailed description of panel a.

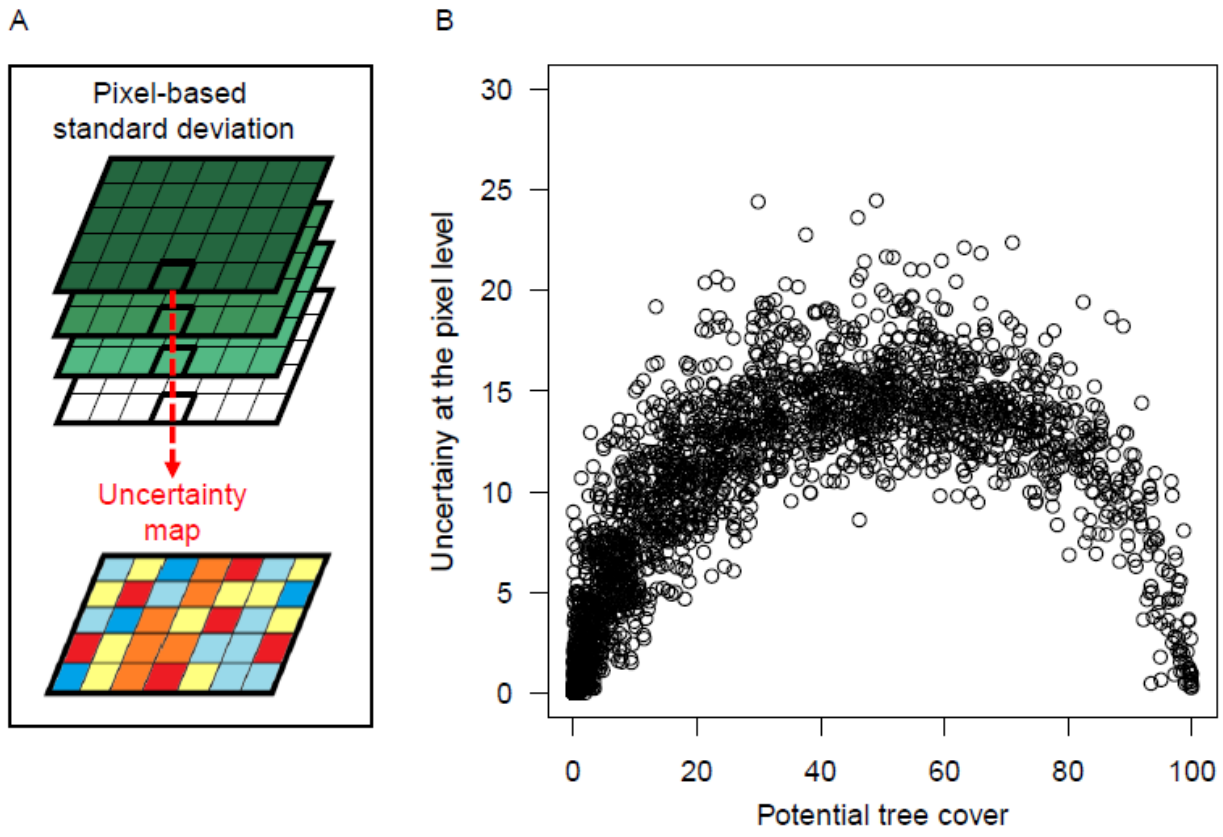

Fig. S5. Uncertainty from k-fold cross validation. The uncertainty is expressed as the standard deviation of the tree cover predicted from the k potential tree cover layers computed during the k-fold cross-validation. (A) Summary of the procedure. (B) Uncertainty (standard deviation) vs. mean predicted tree cover at the pixel level. The relationship shows that the level of uncertainty is greater at intermediate tree cover classes, reaching 15% of tree cover variation at 50% of the predicted potential tree cover.

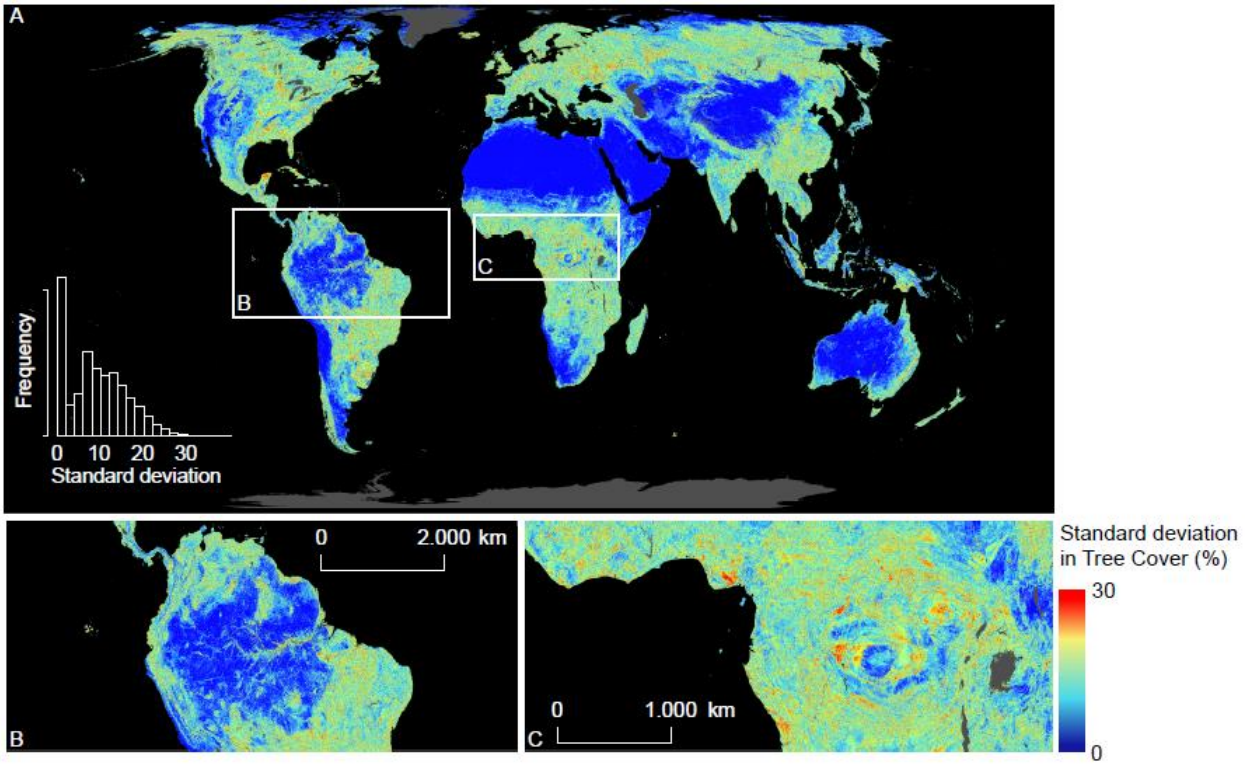

Fig. S6. Uncertainty map of the prediction of potential tree cover. The uncertainty is calculated at the pixel-level as the standard deviation among the k tree cover layers predicted from the k models developed from the k-fold cross-validation. The bimodal distribution of the standard deviation is illustrated within caption (A), showing a peak at 0% and another at 7% of standard deviation in tree cover. The resulting map (A) shows higher uncertainty in regions with intermediate potential tree cover and low uncertainty in regions with low (e.g. desert) or high (rainforest) tree cover levels. One exception remains, with higher levels of uncertainty in tropical wet forests of Central Africa (C) vs. other tropical wet forests (B).

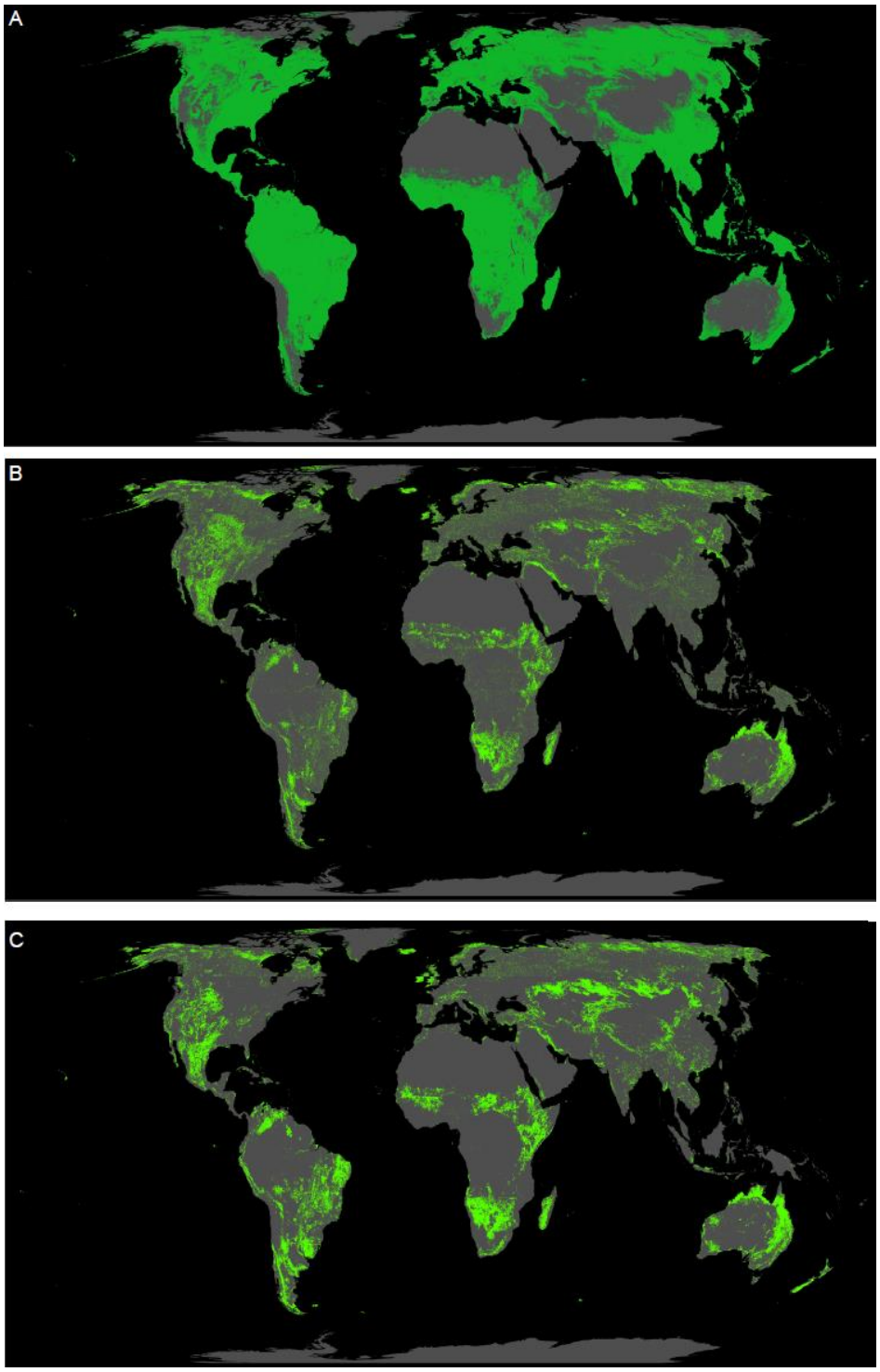

Fig. S7. Global forest restoration potential. The global potential forest cover is illustrated on (A), representing an area of 8.7 billion hectares of forest cover. Forests are defined as pixels with a forest cover ≥ 10%. The global potential forest cover available for restoration is illustrated in (B) using cropland from Globcover and in (C) using Cropland from Fritz and colleagues (2015). These are calculated from the global potential forest cover (A) subtracting existing forest cover and removing agricultural and urban areas. This global tree restoration potential represents an area of 1.8 billion hectares of forest (Globcover; Table S2) or of 1.7 billion hectares of forest (Fritz and colleagues (2015); Table S2).

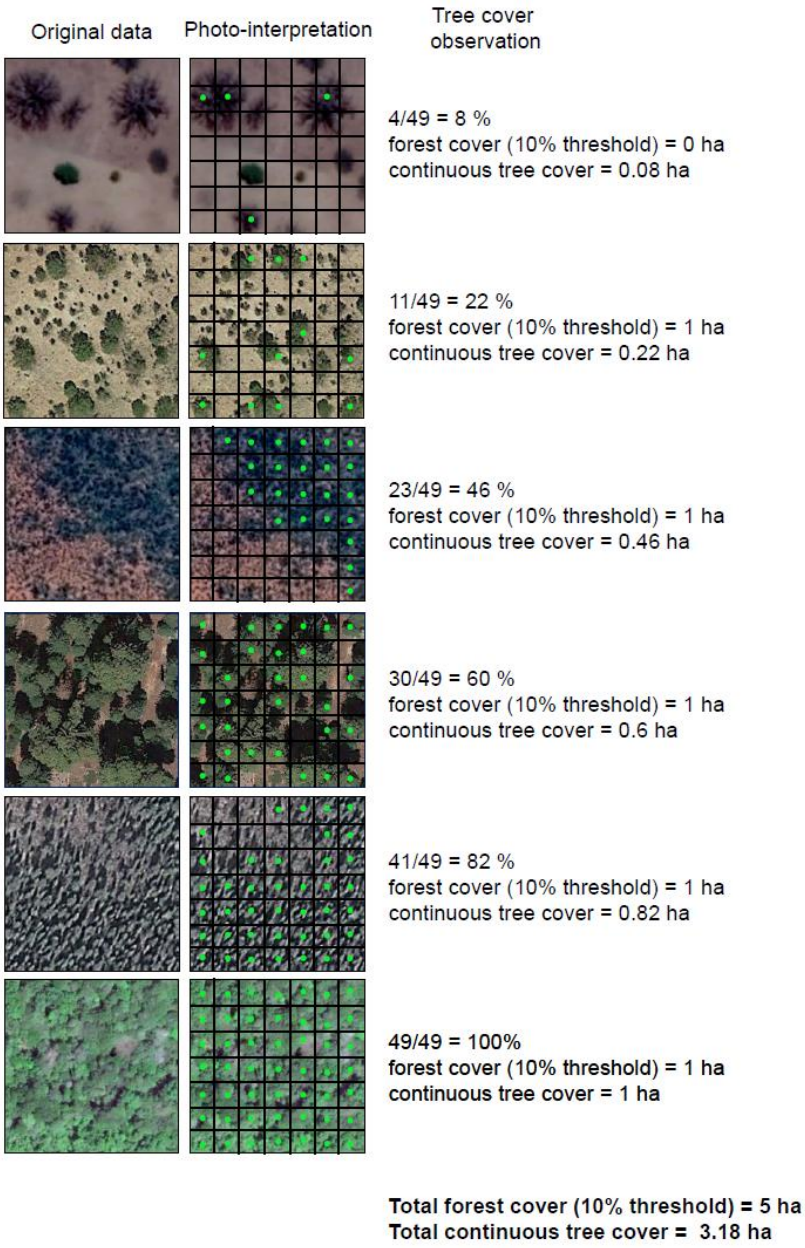

Fig. S8. Principles and calculation of continuous tree cover. Original plots are segmented in 7-by-7 subplots and each cell intercepting a tree crown is scored (green dot). These scores (ranging from 0 to 49 out of 49 subplots) are then used to quantify the tree cover of the plot. The subfigures illustrate that the quantification of the forest cover and of the continuous canopy cover can differ significantly, leading to an overestimation in forest cover area when using a binary forest cover definition. In this example, 36% less forest area was estimated when using continuous canopy cover to calculate forest area.

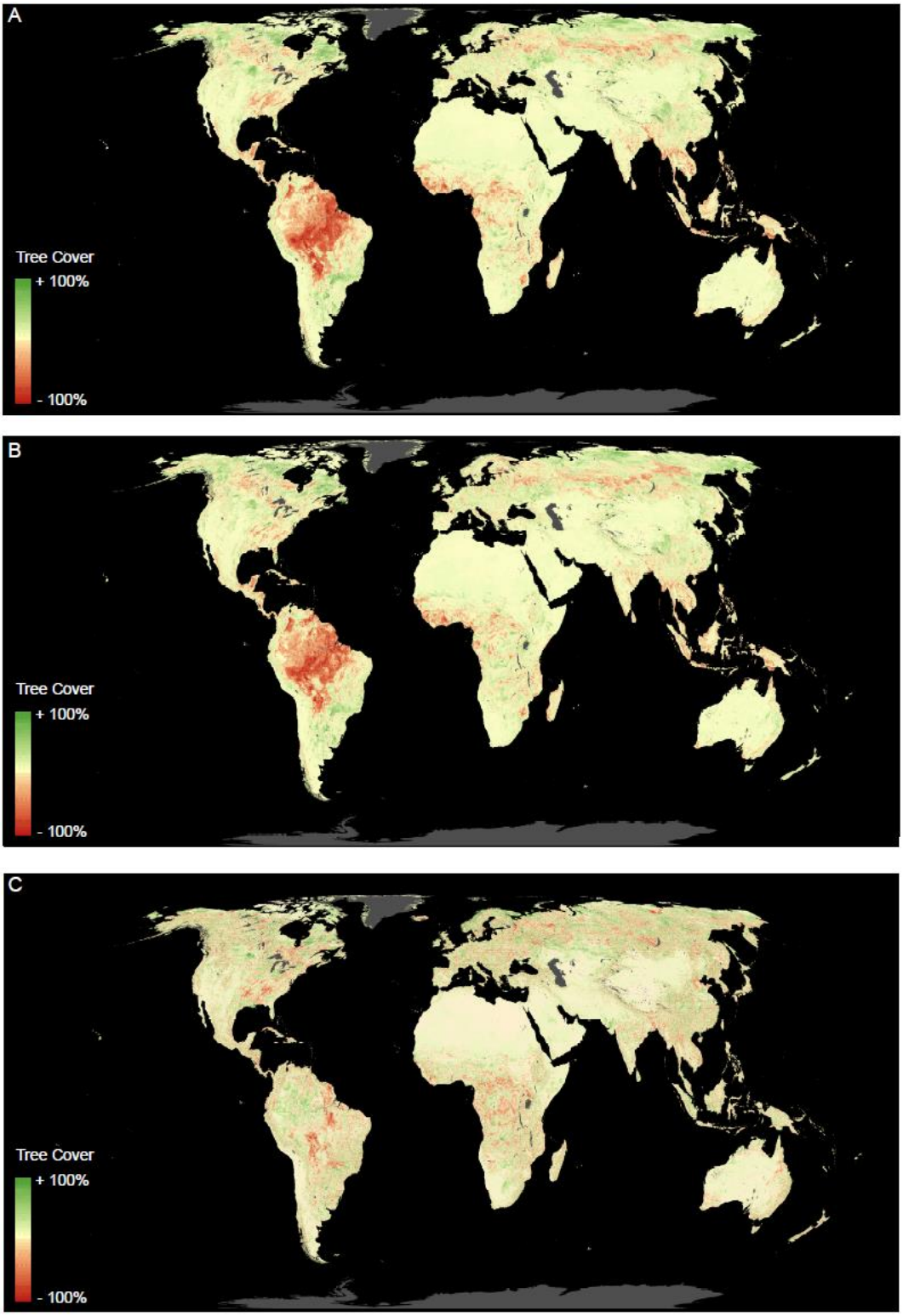

Fig S9. Average expected changes in potential tree cover by 2050. Maps illustrate the average expected changes between current and future conditions of tree cover for three Earth System Models (CESM1-bgc, CESM1-cam5 and mohc-Hadgem2es) and two Representative Circulation Pathways (RCP 4.5 and RCP 8.5). (A) Average expected change according to scenario RCP 4.5. (B) Average expected change according to RCP 8.5. (C) Difference between the two scenarios.

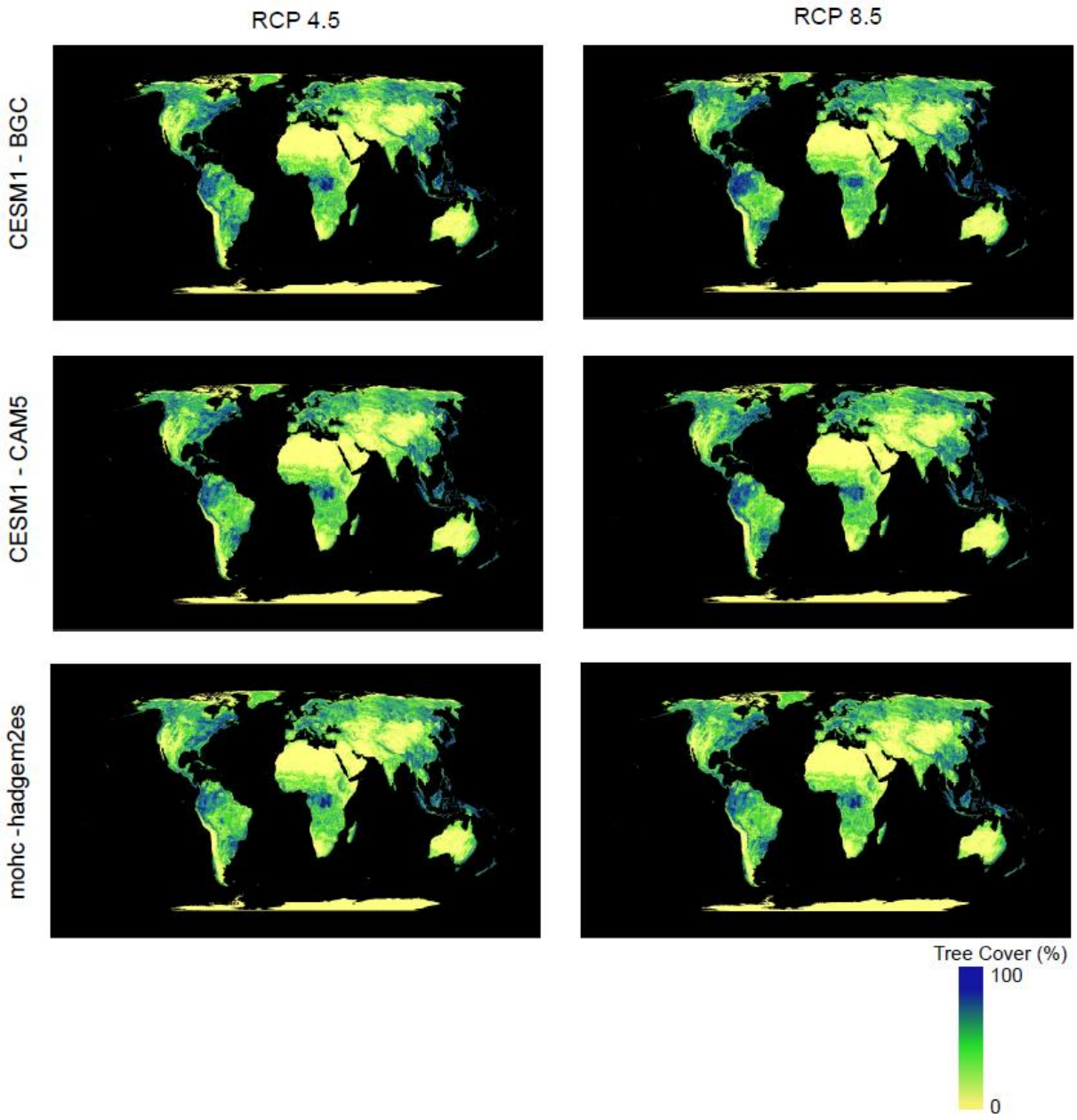

Fig. S10. Potential tree cover in 2050. The extrapolation of the potential tree cover for 2050 is based on the current relationship between tree cover and environmental conditions within the protected areas of the world. Maps are illustrated for three Earth System Models (CESM1-bgc, CESM1-cam5 and mohc-Hadgem2es) and two Representative Circulation Pathways (RCP 4.5 and RCP 8.5).

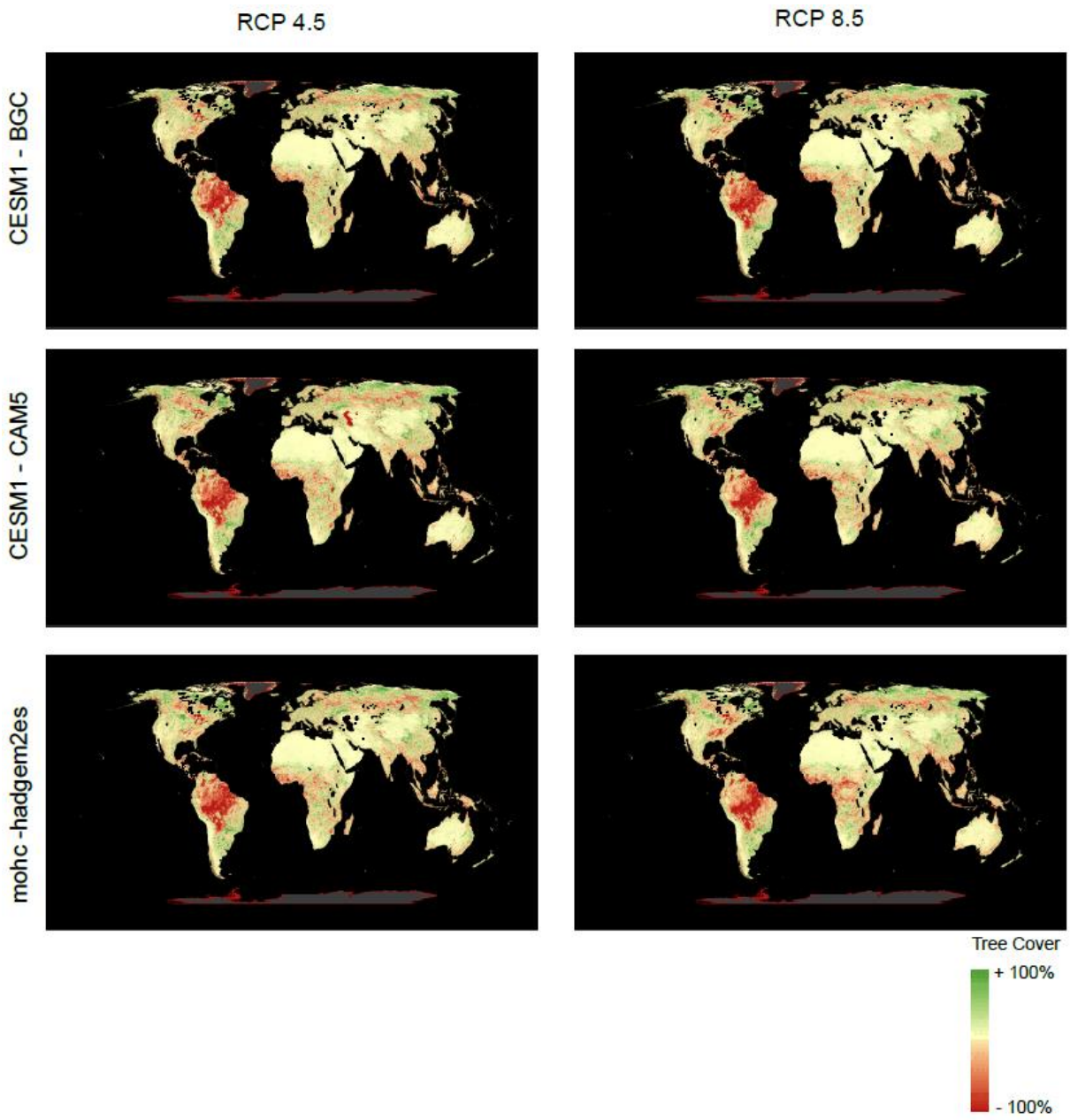

Fig. S11. Expected changes in potential tree cover by 2050. Percentage increase (green) or decrease (red) in potential tree cover by the year 2050 compared to the present. Calculations of changes in the potential tree cover are based on the current relationship between tree cover and environmental conditions within the protected areas of the world. Maps are illustrated for three Earth System Models (CESM1-bgc, CESM1-cam5 and mohc-Hadgem2es) and two Representative Circulation Pathways (RCP 4.5 and RCP 8.5).

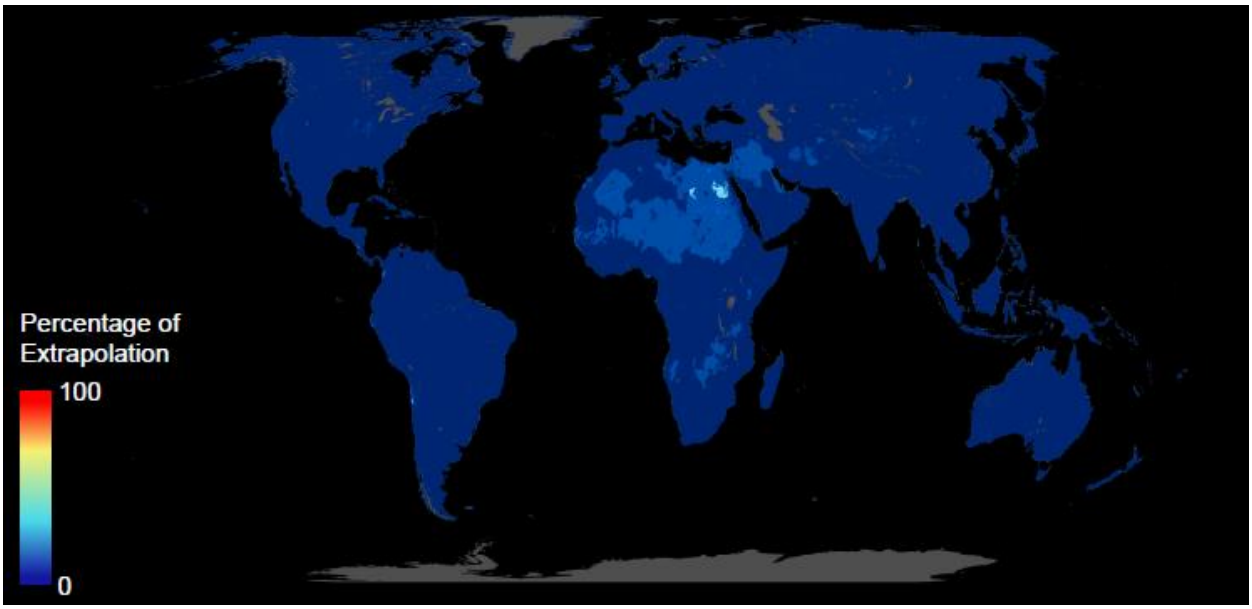

Fig. S12. Interpolation vs. extrapolation of the model. The mean percentage of extrapolation at the pixel level is equal to ~8%, showing that most of the potential tree cover map is interpolated, not extrapolated.

Table S1.

Data Name	Layer Group	Original Spatial Resolution
Latitude / Longitude (Abs_Lat	Abs_Long)	Process
WC01 / BIO01 = Annual Mean Temperature	Climatic	30 arcsec
WC08 / BIO08 = Mean Temperature of Wettest Quarter	Climatic	30 arcsec
WC12 / BIO12 = Annual Precipitation	Climatic	30 arcsec
WC15 / BIO15 = Precipitation Seasonality (Coefficient of Variation)	Climatic	30 arcsec
WC17 / BIO17 = Precipitation of Driest Quarter	Climatic	30 arcsec
Elevation	Topographic	30 arcsec
Hillshade	Topographic	30 arcsec
OCSTHA_M_sd1_250m_ll = Soil Organic Carbon Stock from 0.00m-0.05m	Soil	250m
SNDPPT_M_sl2_250m_ll = Sand content (50â€“2000 micro meter) at 0.05m	Soil	250m
BDRICM_M_1km_ll = Depth to Bedrock	Soil	1km

Table S2. Potential restoration per biome.

	Potential canopy cover (Mha)			Potential forest cover (Mha)			Potential carbon stock		
	total	restoration (Globcover 2009)	restoration (Fritz et al. 2015)	total	Restoration (Globcover 2009)	restoration (Fritz et al. 2015)	density (t.ha-1)	restoration (Globcover 2009; GtC)	restoration (Fritz et al. 2015; GtC)
BIOME									
Tundra	79.1	50.6	50.94	254.9	166.2	508.9	202.4	10.2	10.3
Boreal Forests/Taiga	768.5	178.0	181.8	1493.7	216.0	258.0	239.2	42.6	43.5
Deserts and Xeric Shrublands	129.5	77.6	79.6	413.4	232.7	226.6	202.4	15.7	16.1
Flooded Grasslands and Savannas	25.5	9.0	9.6	69.1	22.9	18.3	202.4	1.8	2.0
Mangroves	14.4	2.6	2.7	27.8	4.4	0.5	282.5	0.7	0.8
Mediterranean Forests	73.2	18.8	15.5	222.4	58.2	3.1	202.4	3.8	3.1
Montane Grasslands and Shrublands	52.9	19.3	22.1	145.9	53.5	41.5	202.4	3.9	4.5
Temperate Broadleaf	615.2	109.0	82.0	1167.4	153.0	39.9	154.7	16.9	12.7
Temperate Conifer Forests	199.8	35.9	34.2	373.2	56.5	134.6	154.7	5.6	5.3
Temperate Grasslands	195.9	72.5	62.7	645.4	243.5	130.7	154.7	11.2	9.7
Tropical Coniferous Forests	32.7	7.1	6.2	63.9	10.6	6.9	282.5	2.0	1.7
Tropical Dry Broadleaf Forests	165.6	32.8	36.2	358.8	50.0	19.5	282.5	9.3	10.2
Tropical Grasslands	569.5	189.5	210.2	1496.8	388.0	164.0	282.5	53.5	59.4
Tropical Moist Broadleaf Forests	1443.8	97.1	117.1	1948.9	115.9	105.1	282.5	27.4	33.1
Total	**4365.5**	**899.9**	**910.7**	**8681.5**	**1771.5**	**1657.4**		**204.7**	**212.3**
Standard deviation (from k-fold crossvalidation)	131.0	27.0	27.3	260.4	53.1	49.7		6.1	6.4

Table S3. Risk of gain and loss in canopy cover per biome by 2050

Ecoregion	RCP4.5 (Mha)	RCP 8.5 (Mha)
Tundra (Boreal)	76.19	101.21
Boreal Forests/Taiga	18.69	26.95
Deserts and Xeric Shrublands	13.49	27.97
Flooded Grasslands and Savannas	-2.77	-3.02
Mangroves	-3.33	-3.47
Mediterranean Forests, Woodlands and Scrub	-1.87	-2.29
Montane Grasslands and Shrublands	20.00	30.90
Temperate Broadleaf and Mixed Forests	-1.11	-4.21
Temperate Conifer Forests	7.29	8.11
Temperate Grasslands Savannas	19.79	32.25
Tropical and Subtropical Coniferous Forests	0.10	0.12
Tropical and Subtropical Dry Broadleaf Forests	-27.98	-46.45
Tropical and Subtropical Grasslands	-18.94	-45.51
Tropical and Subtropical Moist Broadleaf Forests	-278.93	-345.78
SUM	**-174.37**	**-223.19**

Data S1. Photo-interpreted tree cover database
Data S2. Potential restoration by country

References and Notes

1. Intergovernmental Panel on Climate Change (IPCC), *An IPCC Special Report on the Impacts of Global Warming of 1.5 °C Above Pre-Industrial Levels and Related Global Greenhouse Gas Emission Pathways* (IPCC, 2018).

2. B. W. Griscom, J. Adams, P. W. Ellis, R. A. Houghton, G. Lomax, D. A. Miteva, W. H. Schlesinger, D. Shoch, J. V. Siikamäki, P. Smith, P. Woodbury, C. Zganjar, A. Blackman, J. Campari, R. T. Conant, C. Delgado, P. Elias, T. Gopalakrishna, M. R. Hamsik, M. Herrero, J. Kiesecker, E. Landis, L. Laestadius, S. M. Leavitt, S. Minnemeyer, S. Polasky, P. Potapov, F. E. Putz, J. Sanderman, M. Silvius, E. Wollenberg, J. Fargione, Natural climate solutions. *Proc. Natl. Acad. Sci. U.S.A.* **114**, 11645–11650 (2017). doi:10.1073/pnas.1710465114 Medline

3. S. L. Lewis, C. E. Wheeler, E. T. A. Mitchard, A. Koch, Restoring natural forests is the best way to remove atmospheric carbon. *Nature* **568**, 25–28 (2019). doi:10.1038/d41586-019-01026-8 Medline

4. United Nations Environment Programme (UNEP), The Bonn Challenge (2011).

5. UN Climate Summit, New York Declaration on Forests (2014).

6. P. Potapov, L. Laestadius, S. Minnemeyer, *Global Map of Potential Forest Cover* (World Resources Institute, 2011).

7. K.-H. Erb, T. Kastner, C. Plutzar, A. L. S. Bais, N. Carvalhais, T. Fetzel, S. Gingrich, H. Haberl, C. Lauk, M. Niedertscheider, J. Pongratz, M. Thurner, S. Luyssaert, Unexpectedly large impact of forest management and grazing on global vegetation biomass. *Nature* **553**, 73–76 (2018). doi:10.1038/nature25138 Medline

8. A. Bey, A. Sánchez-Paus Díaz, D. Maniatis, G. Marchi, D. Mollicone, S. Ricci, J.-F. Bastin, R. Moore, S. Federici, M. Rezende, C. Patriarca, R. Turia, G. Gamoga, H. Abe, E. Kaidong, G. Miceli, Collect earth: Land use and land cover assessment through augmented visual interpretation. *Remote Sens.* **8**, 807 (2016). doi:10.3390/rs8100807

9. United Nations Educational, Scientific and Cultural Organization (UNESCO), *The World Database on Protected Areas* (UNESCO, 2011).

10. Materials and methods are available as supplementary materials.

11. K. R. Jones, O. Venter, R. A. Fuller, J. R. Allan, S. L. Maxwell, P. J. Negret, J. E. M. Watson, One-third of global protected land is under intense human pressure. *Science* **360**, 788–791 (2018). doi:10.1126/science.aap9565 Medline

12. L. Breiman, Random forests. *Mach. Learn.* **45**, 5–32 (2001). doi:10.1023/A:1010933404324

13. J.-F. Bastin, N. Berrahmouni, A. Grainger, D. Maniatis, D. Mollicone, R. Moore, C. Patriarca, N. Picard, B. Sparrow, E. M. Abraham, K. Aloui, A. Atesoglu, F. Attore, Ç. Bassüllü, A. Bey, M. Garzuglia, L. G. García-Montero, N. Groot, G. Guerin, L. Laestadius, A. J. Lowe, B. Mamane, G. Marchi, P. Patterson, M. Rezende, S. Ricci, I. Salcedo, A. S.-P. Diaz, F. Stolle, V. Surappaeva, R. Castro, The extent of forest in dryland biomes. *Science* **356**, 635–638 (2017). doi:10.1126/science.aam6527 Medline

14. Food and Agriculture Organization (FAO), *Global Forest Resources Assessment 2020: Terms and Definitions* (FAO, 2018).

15. M. C. Hansen, P. V. Potapov, R. Moore, M. Hancher, S. A. Turubanova, A. Tyukavina, D. Thau, S. V. Stehman, S. J. Goetz, T. R. Loveland, A. Kommareddy, A. Egorov, L. Chini, C. O. Justice, J. R. G. Townshend, High-resolution global maps of 21st-century forest cover change. *Science* **342**, 850–853 (2013). doi:10.1126/science.1244693 Medline

16. O. Arino *et al*., *Global Land Cover Map for 2009 (GlobCover 2009)* (European Space Agency, Université catholique de Louvain, PANGAEA, 2012).

17. S. Fritz, L. See, I. McCallum, L. You, A. Bun, E. Moltchanova, M. Duerauer, F. Albrecht, C. Schill, C. Perger, P. Havlik, A. Mosnier, P. Thornton, U. Wood-Sichra, M. Herrero, I. Becker-Reshef, C. Justice, M. Hansen, P. Gong, S. Abdel Aziz, A. Cipriani, R. Cumani, G. Cecchi, G. Conchedda, S. Ferreira, A. Gomez, M. Haffani, F. Kayitakire, J. Malanding, R. Mueller, T. Newby, A. Nonguierma, A. Olusegun, S. Ortner, D. R. Rajak, J. Rocha, D. Schepaschenko, M. Schepaschenko, A. Terekhov, A. Tiangwa, C. Vancutsem, E. Vintrou, W. Wenbin, M. van der Velde, A. Dunwoody, F. Kraxner, M. Obersteiner, Mapping global cropland and field size. *Glob. Chang. Biol.* **21**, 1980–1992 (2015). doi:10.1111/gcb.12838 Medline

18. Y. Pan, R. A. Birdsey, J. Fang, R. Houghton, P. E. Kauppi, W. A. Kurz, O. L. Phillips, A. Shvidenko, S. L. Lewis, J. G. Canadell, P. Ciais, R. B. Jackson, S. W. Pacala, A. D. McGuire, S. Piao, A. Rautiainen, S. Sitch, D. Hayes, A large and persistent carbon sink in the world's forests. *Science* **333**, 988–993 (2011). doi:10.1126/science.1201609 Medline

19. J. Grace, J. Jose, P. Meir, H. S. Miranda, R. A. Montes, Productivity and carbon fluxes of tropical savannas. *J. Biogeogr.* **33**, 387–400 (2006). doi:10.1111/j.1365-2699.2005.01448.x

20. X.-P. Song, M. C. Hansen, S. V. Stehman, P. V. Potapov, A. Tyukavina, E. F. Vermote, J. R. Townshend, Global land change from 1982 to 2016. *Nature* **560**, 639–643 (2018). doi:10.1038/s41586-018-0411-9 Medline

21. U. Büntgen, P. J. Krusic, A. Piermattei, D. A. Coomes, J. Esper, V. S. Myglan, A. V. Kirdyanov, J. J. Camarero, A. Crivellaro, C. Körner, Limited capacity of tree growth to mitigate the global greenhouse effect under predicted warming. *Nat. Commun.* **10**, 2171 (2019). doi:10.1038/s41467-019-10174-4 Medline

22. T. Hengl, J. Mendes de Jesus, G. B. M. Heuvelink, M. Ruiperez Gonzalez, M. Kilibarda, A. Blagotić, W. Shangguan, M. N. Wright, X. Geng, B. Bauer-Marschallinger, M. A. Guevara, R. Vargas, R. A. MacMillan, N. H. Batjes, J. G. B. Leenaars, E. Ribeiro, I. Wheeler, S. Mantel, B. Kempen, SoilGrids250m: Global gridded soil information based on machine learning. *PLOS ONE* **12**, e0169748 (2017). doi:10.1371/journal.pone.0169748 Medline

23. S. E. Fick, R. J. Hijmans, WorldClim 2: New 1-km spatial resolution climate surfaces for global land areas. *Int. J. Climatol.* **37**, 4302–4315 (2017). doi:10.1002/joc.5086

24. G. Piñeiro, S. Perelman, J. P. Guerschman, J. M. Paruelo, How to evaluate models: Observed vs. predicted or predicted vs. observed? *Ecol. Modell.* **216**, 316–322 (2008). doi:10.1016/j.ecolmodel.2008.05.006

25. K.-H. Erb, C. Lauk, T. Kastner, A. Mayer, M. C. Theurl, H. Haberl, Exploring the biophysical option space for feeding the world without deforestation. *Nat. Commun.* **7**, 11382 (2016). doi:10.1038/ncomms11382 Medline

26. J. W. Hurrell, M. M. Holland, P. R. Gent, S. Ghan, J. E. Kay, P. J. Kushner, J.-F. Lamarque, W. G. Large, D. Lawrence, K. Lindsay, W. H. Lipscomb, M. C. Long, N. Mahowald, D. R. Marsh, R. B. Neale, P. Rasch, S. Vavrus, M. Vertenstein, D. Bader, W. D. Collins, J. J. Hack, J. Kiehl, S. Marshall, The Community Earth System Model: A framework for collaborative research. *Bull. Am. Meteorol. Soc.* **94**, 1339–1360 (2013). doi:10.1175/BAMS-D-12-00121.1

27. N. Bellouin, W. J. Collins, I. D. Culverwell, P. R. Halloran, S. C. Hardiman, T. J. Hinton, C. D. Jones, R. E. McDonald, A. J. McLaren, F. M. O'Connor, M. J. Roberts, J. M. Rodriguez, S. Woodward, M. J. Best, M. E. Brooks, A. R. Brown, N. Butchart, C. Dearden, S. H. Derbyshire, I. Dharssi, M. Doutriaux-Boucher, J. M. Edwards, P. D. Falloon, N. Gedney, L. J. Gray, H. T. Hewitt, M. Hobson, M. R. Huddleston, J. Hughes, S. Ineson, W. J. Ingram, P. M. James, T. C. Johns, C. E. Johnson, A. Jones, C. P. Jones, M. M. Joshi, A. B. Keen, S. Liddicoat, A. P. Lock, A. V. Maidens, J. C. Manners, S. F. Milton, J. G. L. Rae, J. K. Ridley, A. Sellar, C. A. Senior, I. J. Totterdell, A. Verhoef, P. L. Vidale, A. Wiltshire, The HadGEM2 family of Met Office Unified Model climate configurations. *Geosci. Model Dev.* **4**, 723–757 (2011). doi:10.5194/gmd-4-723-2011

28. J. Ramirez Villegas, A. Jarvis, Downscaling global circulation model outputs: The delta method decision and policy analysis, Working Paper No. 1 (2010).

29. A. C. Staver, S. Archibald, S. A. Levin, The global extent and determinants of savanna and forest as alternative biome states. *Science* **334**, 230–232 (2011). doi:10.1126/science.1210465 Medline